JACS
JOURNAL OF THE AMERICAN CHEMICAL SOCIETY
Article
pubs.acs.org/JACS

Enhanced Photocurrents with ZnS Passivated Cu(In,Ga)(Se,S)$_2$ Photocathodes Synthesized Using a Nonvacuum Process for Solar Water Splitting

Sang Youn Chae,[†,‡] Se Jin Park,[†,§] Sung Gyu Han,[†,∥] Hyejin Jung,[†,⊥] Chae-Woong Kim,[#] Chaehwan Jeong,[#] Oh-Shim Joo,[†] Byoung Koun Min,[*,†,⊥,▽] and Yun Jeong Hwang[*,†,⊥]

[†]Clean Energy Research Center, Korea Institute of Science and Technology, Seoul 02792, Republic of Korea
[‡]Department of Chemistry, College of Science, Korea University, Seoul 02841, Republic of Korea
[§]Department of Materials Science and Engineering, Korea University, Seoul, 02841, Republic of Korea
[∥]Department of Physics, College of Science, Korea University, Seoul 02841, Republic of Korea
[⊥]Korea University of Science and Technology, Daejeon 34113, Republic of Korea
[#]Applied Optics & Energy R&D Group, Seonam Regional Division, Korea Institute of Industrial Technology, Gwangju 61012, Republic of Korea
[▽]Green School, Korea University, 145, Anam-ro, Seongbuk-gu, Seoul 02841, Republic of Korea

Supporting Information

ABSTRACT: Chalcopyrite Cu(In,Ga)(Se,S)$_2$ (CIGS) semiconductors are potential candidates for use in photoelectrochemical (PEC) hydrogen generation due to their excellent optical absorption properties and high conduction band edge position. In the present research, CIGS thin film was successfully prepared on a transparent substrate (F:SnO$_2$ glass) using a solution-based process and applied for a photocathode in solar water splitting, which shows control of the surface state associated with sulfurization/selenization process significantly influences on the PEC activity. A ZnS passivation surface layer was introduced, which effectively suppresses charge recombination by surface states of CIGS. The CIGS/ZnS/Pt photocathode exhibited highly enhanced PEC activity (~24 mA·cm^{-2} at −0.3 V vs RHE). The performances of our CIGS photocathode on the transparent substrate were also characterized under front/back light illumination, and the incident photon to current conversion efficiency (IPCE) drastically changed depending on the illumination directions showing decreased IPCE especially under UV region with back illumination. The slow minority carrier (electron) transportation is suggested as a limiting factor for the PEC activity of the CIGS photocathode.

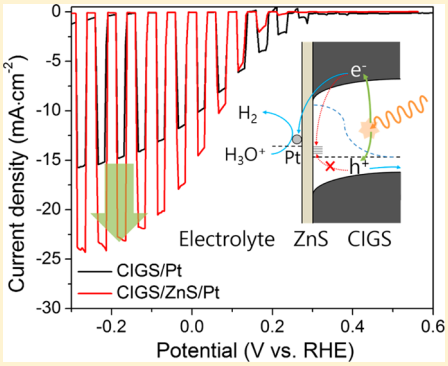

INTRODUCTION

Photoelectrochemical (PEC) water splitting using sunlight has been suggested as a clean method for hydrogen production without the emission of CO_2. Since TiO_2 photoelectrode was demonstrated for PEC water splitting,[1−3] numerous other semiconductor materials have been studied in order to increase solar-to-hydrogen (STH) conversion efficiency and the durability of these cells. However, strict material requirements, such as the suitable electronic band positions, size of band gap (E_g = 1.8−2.0 eV), and resistance to decomposition, limit the available choices of semiconductor materials. Some visible light absorbers such as Cu_2O or Ta_3N_5 have suitable band positions for spontaneous water splitting[4,5] but are very unstable during the PEC reaction.[4,6,7] It is thus very difficult to achieve a highly active spontaneous water splitting system with a single PEC material.

Therefore, a photodiode system composed of an n-type photoanode and a p-type photocathode has been suggested to reduce the aforementioned limitations and increase STH efficiency.[8] In a photodiode system, the band gap of the semiconductor can be smaller than 1.23 eV, and its valence or conduction band can be located outside of the water redox potential because each photoelectrode is allocated only water oxidation or reduction. As a result of this, more options for semiconductor materials become available.[9−11] Recent studies have reported progressive improvement with n-type semiconductors such as WO_3, Fe_2O_3, and $BiVO_4$, and many of them can be fabricated using a low-cost solution process.[12−14] However, compared with n-type semiconductors, p-type semiconductors have received less attention. Si, Cu_2O, and III−V group semiconductors (e.g., p-GaN, InP, and GaAs) have been studied for use in solar hydrogen production,[15−17] but further material development is essential to improve durability and ensure cost-effective preparation for practical water splitting applications.

Received: September 13, 2016
Published: November 8, 2016

DOI: 10.1021/jacs.6b09595
J. Am. Chem. Soc. 2016, 138, 15673−15681

Copper indium gallium selenide ($Cu(In,Ga)Se_2$, CIGS) is a particularly interesting visible light absorber due to its easy band gap tuning[18] and high absorption coefficient ($\sim 10^5 \times cm^{-1}$).[19] There have been a number of studies conducted on potential photovoltaic (PV) cell applications but little research into PEC water splitting because the small CIGS band gap cannot fulfill the overall water splitting. However, it can be combined with other semiconductor materials, and its high conduction band minimum is promising for use in a photocathode as it facilitates electron transfer from CIGS to the hydrogen evolution reaction without external bias potential.[7] Diverse research on preparation methods, substrates, surface buffer layers, cocatalysts, and stability should be conducted in relation to the application of CIGS in solar water splitting to improve its activity and stability. Unlike PV cells, PEC cells deal with minority carrier transfer at the semiconductor-electrolyte junction, so photogenerated electron transfer at the CIGS surface needs to be prioritized as a research focus.

As an alternative to vacuum processes (e.g., coevaporation or sputtering),[20−22] various solution process methods (e.g., nanoparticle, electrodeposition, and chemical solution synthesis)[23−25] have recently been developed for the preparation of CIGS thin film with the goal of cost-effective, and large scale production. However, lower PEC activity has been reported because solution processes produce poor crystal quality (i.e., small grains or undesirable binary compounds), resulting in CIGS film with a short lifetime as a charge carrier.[26,27] Preventing crystal defects and controlling surface states are particularly important for solution-processed CIGS in PEC applications.

In this study, we develop a solution-process-based thin-film photocathode for solar water splitting with sulfur-containing CIGS ($Cu(In,Ga)(Se,S)_2$) and include a ZnS surface layer to improve the photocurrent of the CIGS photocathode. Typically, a CdS buffer layer is used in CIGS photocathodes because the p−n junction can enhance charge separation efficiency and shift the onset potential of the photocurrent toward the anodic potential.[28] However, CdS is unstable during PEC reactions in aqueous media and the toxicity of cadmium is of concern.[21] Therefore, developing a new surface layer is required for CIGS photocathodes that are intended to be used in PEC applications. We demonstrate the role of the ZnS layer on the CIGS surface in retarding electron−hole recombination.

Here, a transparent substrate (fluorine-doped tin oxide, FTO) was used for the CIGS photocathode. Transparency is beneficial when attempting to characterize PEC performance and can also be used in a tandem or dual absorber system because it allows bidirectional (i.e., front/back) illumination. Unfortunately, however, most CIGS thin films are developed on an opaque Mo sputtered glass substrate because of the ohmic contact. Because we prepare CIGS thin film on a transparent FTO substrate, the PEC activity of CIGS can be measured for both front and back illumination, which suggests that electron transportation limits the charge separation efficiency of CIGS photocathodes.

EXPERIMENTAL SECTION

CIGS Thin Film Preparation. CIGS thin film was synthesized on an FTO-coated glass substrate (Pilkington, TEC 7) or simple soda-lime glass by modifying a previous spin-coating method.[29] To begin with, 0.82 g $Cu(NO_3)_2{\cdot}xH_2O$ (Sigma-Aldrich, 99.999%,), 1.12 g $In(NO_3)_3{\cdot}xH_2O$ (Sigma-Aldrich, 99.99%), 0.41 g $Ga(NO_3)_3{\cdot}xH_2O$ (Sigma-Aldrich, 99.999%), and polyvinyl acetate (Sigma-Aldrich, 1.0 g) were mixed in 17 mL methanol. This precursor solution was spin-coated on clean FTO or soda-lime glass at 2000 rpm for 40 s and annealed at 300 °C for 30 min. The spin-coating and annealing process was repeated several times to obtain the desired film thickness (400, 600, 800 nm, or 1 μm). The film was then sulfurized/selenized in a tube furnace into which a 0.54 g Se pellet (Sigma-Aldrich, 99.99%) had been put to generate Se vapor and through which H_2S (1%)/Ar flowed. Two different concentrations of S in the CIGS were prepared using variations in the sulfurization/selenization process. For the low S concentration (denoted by CIGS-A), the sample was annealed at 500 °C for 10 min with Se vapor and H_2S (1%)/Ar gas flow. For the high S concentration (denoted by CIGS-B), the sample was treated at 500 °C for 30 min under the same Se vapor and H_2S (1%)/Ar gas flow and then treated further at 540 °C for 10 min. Following the sulfurization/selenization process, binary chalcogenide impurities were chemically etched by dipping the sample in 0.5 M KCN for 1 min.

ZnS Layer and Pt Cocatalyst Deposition. ZnS was deposited on the prepared CIGS film using a solution process. The CIGS film was dipped alternately in aqueous solutions of 0.1 M $Zn(CH_3COO)_2{\cdot}2H_2O$ (Junsei, 99%) and 0.1 M $Na_2S{\cdot}9H_2O$ (Sigma-Aldrich, 98%) for 1 min, respectively. This dipping process was repeated for 30 cycles to ensure a uniform coating on the CIGS surface. The platinum cocatalyst was electrochemically deposited in an aqueous solution of 1 mM $H_2PtCl_6{\cdot}6H_2O$ (Sigma-Aldrich, 37.5% Pt basis) with a Pt counter electrode and an Ag/AgCl reference electrode. The Pt deposition conditions were adjusted for CIGS-A, CIGS-B, and CIGS/ZnS films to ensure the working electrodes had the highest possible photocurrent density. For example, −0.12 V vs Ag/AgCl was applied for 120 s to CIGS-A, −0.15 V vs Ag/AgCl for 180 s to CIGS-B film, and −0.15 V vs Ag/AgCl for 675 s to CIGS/ZnS films.

Photoelectrochemical and Electrochemical Characterization. The PEC characterization of the CIGS photocathodes was performed based on linear sweep voltammetry (LSV; 10 $mV{\cdot}s^{-1}$) using a potentiostat (Iviumstat) with a three-electrode configuration in 0.5 M of H_2SO_4 aqueous electrolyte (pH 0.91). All of the three-electrode measurements were carried out with the Pt counter and Ag/AgCl reference electrodes. The measurement was conducted in simulated sunlight (100 $mW{\cdot}cm^{-2}$) from a solar simulator (ABET, Sun 2000) equipped with a 300 W xenon lamp and an AM 1.5 filter, and the incident light was chopped during LSV measurement. The open circuit voltage of the CIGS PEC cell was measured using chronopotentiometry. The measured applied potentials were converted to a reversible hydrogen electrode (RHE) following eq 1:

$$E_{RHE} = E_{Ag/AgCl} + (0.0591\ pH) + E^0{}_{Ag/AgCl}$$

$$E^0{}_{Ag/AgCl}(3M\ NaCl) = 0.209V \text{ at } 25°C \quad (1)$$

To measure the incident photon-to-current conversion efficiency (IPCE), incident light was generated from a 1000 W xenon lamp coupled with an IR water filter and a motorized monochromator (Newport, Cornerstone 130). The IPCE was calculated using eq 2:

$$\text{IPCE}\ (\%) = \frac{I_{ph}(mA{\cdot}cm^{-2}) \times 1239.8(V{\cdot}nm)}{P_{mono} \times \lambda(nm)} \times 100\% \quad (2)$$

where I_{ph} is the steady-state photocurrent at −0.5 V vs Ag/AgCl, λ is the wavelength of the incident light, P_{mono} is the light intensity of each wavelength measured by a calibrated reference Si photodiode.

The Mott−Schottky measurements were also carried out in a 0.5 M H_2SO_4 electrolyte without light irradiation in the frequency range of 50−3000 Hz.

Gas Quantification. The photocurrent of the CIGS photoelectrode was measured using chronoamperometry at 0.5 V vs Ag/AgCl under the same simulated sunlight irradiation. A polyether-etherketone (PEEK) electrochemical cell equipped with a quartz window was designed to connect a gas chromatography (GC; Younglin 6000) for online analysis. The gas products from the CIGS photoelectrodes were analyzed using GC during photocurrent

DOI: 10.1021/jacs.6b09595
J. Am. Chem. Soc. 2016, 138, 15673−15681

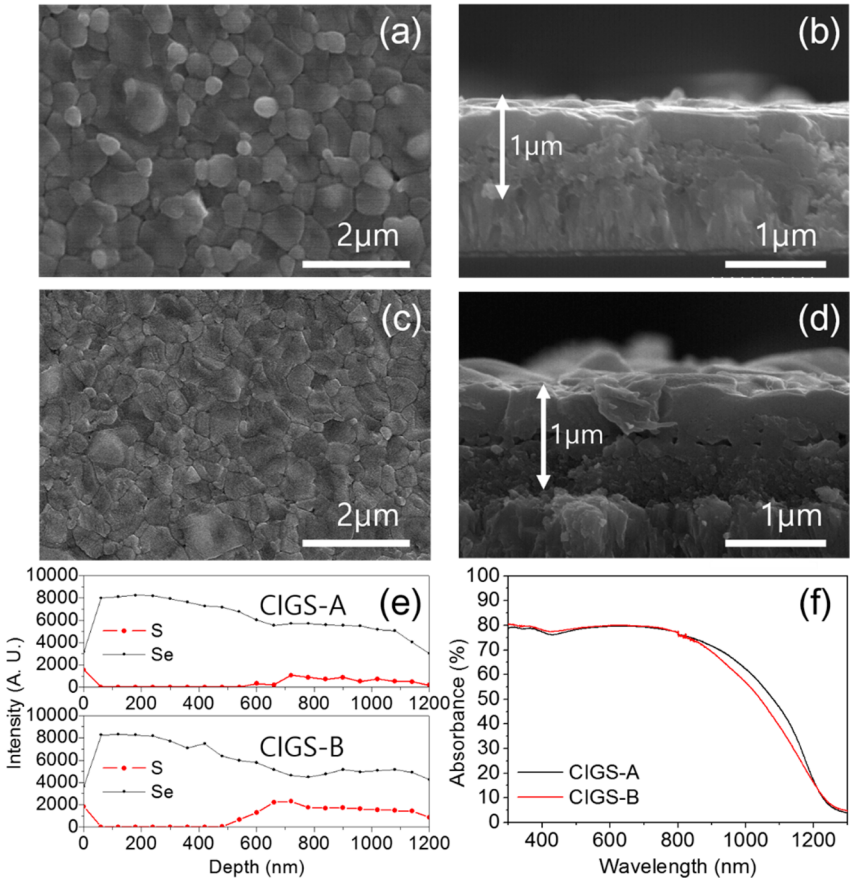

Figure 1. Characterization of CIGS-A and CIGS-B. Surface and cross sectional SEM images of CIGS-A (a,b), and CIGS-B (c,d) thin film on the FTO substrate. (e) XPS depth profile of CIGS thin films, and (f) their absorbance spectra.

measurement. The GC utilized a capillary column (Restek, RT-Msieve 5A) and a pulsed discharge ionized detector (PDD). Ultrahigh purity He gas (99.9999%) was used as a carrier gas and the gas products were directly injected through a six-port valve with a 120 $cm^3 \cdot sec^{-1}$ continuous flow rate, confirmed by a universal flow meter (Agilent Technologies, ADM 2000). The concentration of the produced hydrogen gas was quantified using a gas chromatogram and its current efficiency (i.e., Faradaic efficiency; FE) was obtained using eq 3:

$$\mathrm{FE}_{\mathrm{H}_2}(\%) = \frac{2Fp}{RTJ_{\mathrm{ph}}} \times V_{\mathrm{H}_2} \times Q \times 100 \tag{3}$$

where F is the Faraday constant (96485 $A \cdot s \cdot mol^{-1}$), p is the pressure, R is the ideal gas constant (8.314 $J \cdot mol^{-1} \cdot K^{-1}$), and T is the temperature (in this case, room temperature), J_{ph} is the photocurrent during chronoamperometry under light illumination, V_{H_2} is the volumetric concentration of H_2 from the gas chromatogram, and Q is the flow rate (120 $cm^3 \cdot sec^{-1}$).

Material Characterization. Scanning electron microscopy (SEM; Hitachi, S-4100) was used to measure the morphology and energy-dispersive X-ray spectroscopy (EDS) of the photocathodes. An ultraviolet−visible−near-infrared (UV−vis−NIR) spectrometer (Varian, Cary 5000) was used to confirm the optical properties of the CIGS thin film. The penetration depth of the CIGS thin film was calculated from the reciprocal of the absorption coefficient, which was obtained from the optical properties using UV−vis−NIR spectroscopy. The absorption coefficient was calculated with eq 4:

$$\alpha = \frac{1}{d}\ln\left\{\frac{(1-R)^2}{2T} + \sqrt{\frac{(1-R)^2}{2T} + R^2}\right\} \tag{4}$$

where α is the absorption coefficient, T is the transmittance, R is the reflectance, and d is the thickness of the film measured from a cross-sectional SEM image. X-ray diffraction (XRD) (Shimadzu, XRD-6000) was carried out to characterize the crystal structure of the CIGS thin film.

The elementary composition of the CIGS thin film and ZnS-coated CIGS was measured using X-ray photoelectron spectroscopy (XPS; ULVAC PHI, PHI 5000 VersaPorobe). The recombination processes in the CIGS and ZnS coated CIGS thin film were investigated by using time-resolved photoluminescence (TR-PL; Hammatsu C12132).

RESULTS AND DISCUSSION

Two types of CIGS film (CIGS-A and CIGS-B) with differing sulfur incorporation were prepared by adjusting selenization/sulfurization condition. The SEM images (Figure 1, a−d) show that these CIGS thin films produced from the solution process on the FTO substrate were dense without a porous structure, similar to a previous study, and CIGS-B had a rougher surface.[29] The grain sizes of the prepared films were several hundred nanometers with ∼1 μm thickness. Almost identical XRD patterns were obtained from the CIGS-A and CIGS-B film, indicating the same crystalline structures (JCPDS No. 04−017−0346; Figure S1, Supporting Information).

XPS depth profiles were constructed to distinguish the amount of S incorporated into the CIGS-A and CIGS-B film (Figure 1e and Figure S2), and higher S incorporation was found at the bottom of the CIGS-B film compared to that of the CIGS-A film due to the longer H_2S gas treatment time applied during the sulfurization/selenization process. A higher S ratio in CIGS can increase the band gap and thus affect its

DOI: 10.1021/jacs.6b09595
J. Am. Chem. Soc. 2016, 138, 15673−15681

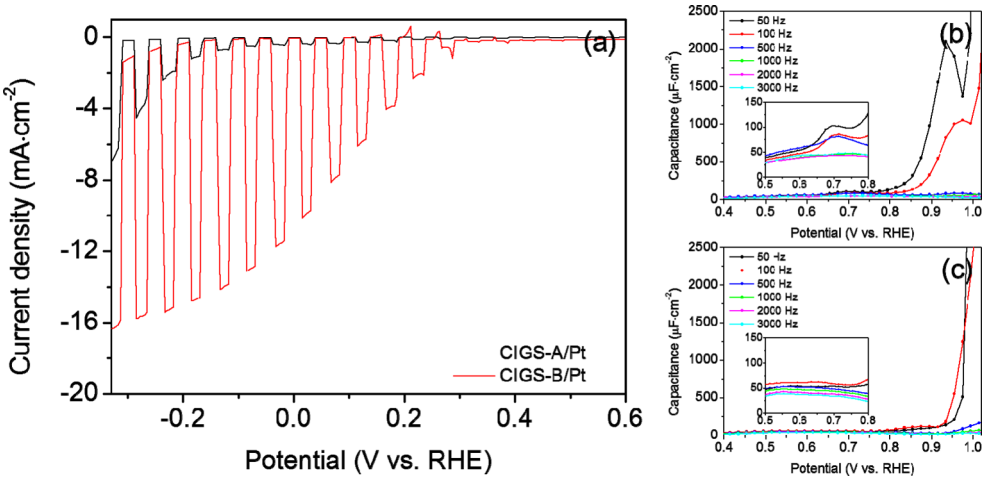

Figure 2. (a) $I-V$ curves of Pt loaded CIGS thin film photocathodes under chopping the simulated sunlight, and capacitance−potential curves of (b) CIGS-A and (c) CIGS-B electrode measured in dark condition by varying the applied frequencies.

light absorption properties.[30] On the other hand, a In/Ga atomic ratio is similar for both CIGS-A and CIGS-B because the same metal precursor solution was used during spin coating (Figure S2, Supporting Information).

To analyze the absorption properties of the synthesized CIGS film, a simple soda-lime glass was used as an alternative substrate to prevent any interference with the FTO thin film. As expected from the higher S concentration, CIGS-B film demonstrated a slight decrease in absorbance in the near IR light region compared to CIGS-A (Figure 1f), but this difference was not significant. The CIGS-B thin film showed small blue shift (0.02 eV) in the emission of PL compared to CIGS-A thin film (Figure S3, Supporting Information). As a result, we found that the additional H_2S treatment in our synthesis method affected the amount of S incorporated into the CIGS film, resulting in slight changes in morphology and an increase in the band gap.

Despite the minor nature of these changes, the prepared CIGS-A and CIGS-B thin films exhibited remarkable differences in PEC water splitting performance. A Pt cocatalyst was applied to each CIGS film to measure reduction activity. Both types of CIGS thin film electrode produced a cathodic photocurrent under chopped light irradiation (Figure 2a). The presence of a cathodic photocurrent indicates that the synthesized CIGS thin film is acting as a p-type semiconductor in the hydrogen evolution reaction. In a comparison of the photocurrent densities of the two CIGS films, CIGS-B film showed an almost 30 times higher photocurrent at a given bias potential (0 V vs RHE). Multiple factors, such as sunlight absorption capability, charge separation, and the potential of the band edge, can affect the final photocurrent density. As we mentioned earlier, according to the UV−vis−NIR and PL emission spectra, the difference between the light absorption properties of CIGS-A and CIGS-B were minimal. Therefore, light absorption is not the primary factor explaining the large discrepancy in photocurrent density.

To understand the increase in PEC activity observed in CIGS-B film, the band potential of each CIGS thin film underwent Mott−Schottky analysis (Figure S3a,b, Supporting Information). The potential of the conduction band edge or the flat band potential is important in allowing thermodynamic electron flow from the CIGS photocathode to the electrolyte in the spontaneous hydrogen evolution reaction. The Mott−Schottky measurements found that the flat band potential of the two types of CIGS film was similar (0.49 and 0.43 V vs RHE for CIGS-A and CIGS-B, respectively). The flat band potential difference may be caused by In/Ga and S/Se atomic ratio difference between CIGS-A and CIGS-B. From the slopes of Mott−Schottky plots, the measured charge carrier densities were 1.24×10^{17} cm^{-3} (CIGS-A) and 4.66×10^{16} cm^{-3} (CIGS-B) whose difference was not significant. Additionally the open circuit potential (V_{oc}) of the two was similar under illumination (Figure S4, Supporting Information). Consequently, neither V_{oc} nor flat band potential can explain the large photocurrent increase in CIGS-B film.

On the other hand, CIGS-A and CIGS-B differed significantly in their capacitance−potential curves (Figure 2b,c) for various frequencies, which is related to the surface states of the two films. Capacitance−potential curves are widely used to investigate the charge transfer behavior at Schottky junctions, including at the semiconductor electrode/electrolyte interface. With the assumption that the capacitance of the Helmholtz layer at the electrode/electrolyte interface is sufficiently larger than that of the space charge region at the semiconductor surface, the capacitance of the semiconductor and voltage ideally follows the Mott−Schottky relationship depicted in eq 5:

$$\frac{1}{C^2} = \frac{2}{\epsilon\epsilon_0 e N_D}\left(E - E_{fb} - \frac{kT}{e}\right) \quad (5)$$

where C is the capacitance of the semiconductor, ϵ is the dielectric constant of the semiconductor, ϵ_0 is the vacuum permittivity, e is the elementary charge, k is the Boltzmann constant, T is the temperature, N_D is the charge carrier density in the semiconductor, E is the applied potential, and E_{fb} is the flat band potential of the semiconductor. However, if the semiconductor has surface states, interface states, or defects, the Mott−Schottky relationship deviates from the ideal linear relationship because these surface states contribute to extra capacitance, resulting in peaks in the capacitance−potential curve.[31−33]

The CIGS-A film had two peaks at 0.70 and 0.95 V vs RHE in the low frequency regions of 50 and 100 Hz (Figure 2b). The disappearance of these peaks in the high frequency regions over 1 kHz suggests again that they are related to surface states because the complete charging of these surface states can be

DOI: 10.1021/jacs.6b09595
J. Am. Chem. Soc. 2016, 138, 15673−15681

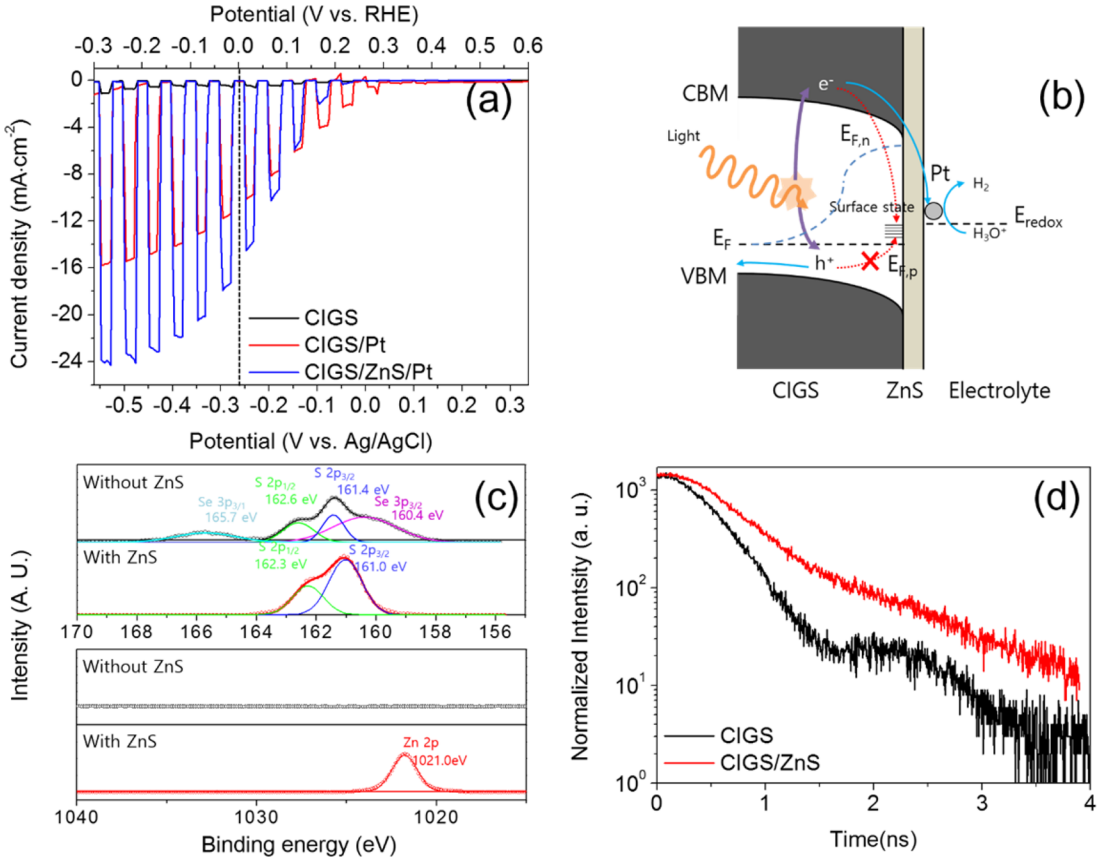

Figure 3. (a) *I*–*V* curves of CIGS, CIGS/Pt and CIGS/ZnS/Pt photocathodes, and (b) a schematic diagram showing charge flow under light illumination. (c) XPS spectra of Zn 2p and S 2p before/after ZnS layer coating on a CIGS photocathode, and (d) time-resolve photoluminescence measured with CIGS and CIGS/ZnS photocathode showing slow decay after ZnS layer coating.

prevented at high frequencies, and thus the interface would behave more classically.[33] On the other hand, smooth capacitance–potential curves were obtained with the CIGS-B film for all applied frequencies. This indicates that CIGS-A may have more surface states than CIGS-B, which can act as recombination centers that are detrimental for the efficient separation of charge in the photoelectrodes. Therefore, the difference in surface states might explain the increase in PEC activity in CIGS-B photocathodes, although further studies are required to understand how the sulfurization/selenization process can influence on the surface states. Generally, solution-processed CIGS film has been reported to be vulnerable to defects or the formation of more grain boundaries and thus exhibits a poor photoresponse. Unlike CIGS film prepared by the well-established vacuum process, synthesizing homogeneous, high crystalline CIGS thin film via a solution-based process remains challenging.[26,27,34] Our solution-processed CIGS-B thin film photocathode demonstrated that photocathodic activity can be greatly enhanced by adjusting S incorporation process. We thus focused on CIGS-B film (denoted as simply CIGS hereafter) for the analysis of PEC activity in the remainder of this paper.

The surface modification of photoactive material is a promising method for further enhancing the photocathodic performance of CIGS film. Surface treatment with an additional coating layer has been demonstrated to protect the semiconductor from corrosion and to suppress surface recombination.[35] We applied a wide band gap material, ZnS, as a passivation layer because it absorbs only the UV region of solar light. ZnS passivation layers have been demonstrated to suppress the recombination of electron–hole pairs in quantum dot sensitized solar cells.[36–40]

A ZnS thin film was coated onto the CIGS thin film using a simple solution process at room temperature and the photocurrent densities of CIGS thin film were compared for bare CIGS, CIGS/Pt, and CIGS/ZnS/Pt photocathodes (Figure 3). When ZnS and Pt were loaded, however, the photocurrents dramatically rose for both CIGS-A and CIGS-B (Figure 3a, and Figure S5, Supporting Information). The charge flow under illumination is expected as shown in Figure 3b. The photocurrent density improved from ∼10.5 mA·cm^{-2} to ∼16 mA·cm^{-2} at 0 V vs RHE with the addition of a ZnS surface layer. The photocurrent density with a CIGS/ZnS/Pt photocathode increased even further, up to ∼24 mA·cm^{-2} at −0.3 V vs RHE, which is noticeably higher than other CIGS photocathodes produced via solution processes. Table 1 summarizes the photocurrent and measurement conditions for previously reported CIGS photocathodes. Most of the CIGS photocathodes fabricated using solution processes such as spin coating, electrodeposition, or nanoparticle synthesis produce a photocurrent of 5–8 mA·cm^{-2} at 0 V vs RHE. The photocurrent density in the present study is thus comparable to the most effective CIGS photocathodes prepared using the more expensive vacuum process (i.e., the coevaporation method). Therefore, the results of the present study demonstrate that highly active CIGS photocathodes can be also manufactured using a cost-effective solution process.

DOI: 10.1021/jacs.6b09595
J. Am. Chem. Soc. 2016, 138, 15673–15681

Table 1. PEC Activity Comparison of Reported Chalcopyrite Photocathodes for Water Splitting[a]

material	interface/cocatalyst	process	deposition method	substrate	photocurrent ($mA \cdot cm^{-2}$)	electrolyte	ref.
$Cu(In,Ga)(S,Se)_2$	CIGSSe/ZnS/Pt	Solution process	Spin coating	FTO glass	−16 (−24 at −0.3 V vs RHE)	0.5 M H_2SO_4 (pH 0.91)	This work
$Cu(In,Ga)Se_2$	CIGSe/CdS		Electrodeposition	Mo/Glass	−8 (at −0.4 V vs SCE)	0.5 M Na_2SO_4	24
$Cu(In,Ga)Se_2$	CIGS/CdS/Pt		Spin coating	FTO glass	−6	0.2 M Na_2HPO_4 (pH 10)	25
$Cu(In,Ga)S_2$	CIGS/CdS/Pt		Spray deposition	Mo/Glass	−6.78	0.1 M Na_2SO_4 (pH 9)	46
$Cu(In,Ga)S_2$	Sb:CIGS/CdS/TiO_2/Pt		Nanoparticle	Mo foil	−5	0.5 M NaS_2O_4 0.25 M Na_2HPO_4 0.25 M NaH_2PO_4 (pH 6.1)	23
$CuInS_2$	Bi:CIS/CdS/TiO_2/Pt		Nanoparticle	Mo foil	−8	0.5 M NaS_2O_4 0.25 M Na_2HPO_4 0.25 M NaH_2PO_4 (pH 6.1)	23
$CuInS_2$	$CuInS_2$/CdS/TiO_2/Pt		Electrodeposition	Mo/Glass	−13	0.1 M Na_2HPO_4 (pH 10)	47
$CuInS_2$	CIGSe/CdS/Pt	Vacuum process	Coevaporation	Mo/Glass	−12	0.1 M Na_2SO_4 (pH 9)	28
$Cu(In,Ga)Se_2$	CIGSe/CdS/ZnO/Pt		Coevaporation	Mo/Glass	−6 (at −0.6 V vs NHE)	0.5 M H_2SO_4	20
$Cu(In,Ga)Se_2$	CIGSe/CdS/Ti/Mo/Pt		Coevaporation	Mo/Glass	−30	Phosphate buffered 0.5 M Na_2SO_4 (pH 6.8)	21
$Cu(In,Ga)Se_2$	CIGSe/Pt:TiO_2		Coevaporation	Mo/Glass	−15	0.5 M H_2SO_4 (pH 0.3)	48
$Cu(In,Ga)Se_2$	CIGSe/CdS/i-ZnO/Al:ZnO/Pt		DC-sputtering	Stainless steel	−30	0.5 M H_2SO_4	49
$Cu(In,Ga)Se_2$	CIGSe/CdS/i-ZnO/Al:ZnO/Pt		Coevaporation	Mo/Glass	−32.5	0.5 M Ns_2SO_4 (pH 9)	50
$Cu(In,Ga)Se_2$	CIGSe/CdS/ZnO/TiO_2/Pt		Coevaporation	Mo/Glass	−34	0.5 M H_2SO_4 (pH 0)	21

[a]Photocurrent values were compared at 0 V vs RHE.

Furthermore, it is obvious that the control of surface states is critically important to the improvement in PEC performance.

On the other hand, the onset potential of the photocurrent was shifted cathodically by 100 mV after the ZnS layer was coated onto the CIGS film, which indicates that the electron transfer from CIGS to ZnS was not facile. This might be because the conduction band minimum (CBM) of ZnS is more negative than the CBM of CIGS, which can lead to the formation of a barrier at the interface. However, steeper band bending allows electron transfer though the ZnS thin film when more cathodic potential is applied.

The successful deposition of the ZnS layer was confirmed with SEM (Figure S6, Supporting Information), and XPS element analysis showed that the top surface was completely covered by ZnS. After the addition of the ZnS layer to the CIGS film, Cu $2p_{3/2}$, In $3d_{5/2}$, and Se 3d signals were totally suppressed (Figure S7, Supporting Information). In addition, Zn $2p_{3/2}$ signals were observed at a binding energy of 1021.0 eV only after ZnS coating. We also observed a change in the S 2p spectra (Figure 3c). The spectra for Se 3p and S 2p overlapped for the bare CIGS film in a manner similar to previously reported XPS spectra.[41] However, with the addition of the ZnS layer, the Se 3p signals disappeared and only S $2p_{3/2}$ (161.9 eV) and S $2p_{3/1}$ (161.0 eV) binding energies were observed. All of the Zn and S signals indicate the chemical state of ZnS.[42,43]

To understand the contribution of ZnS, photoexcited charge carrier kinetics were investigated using time-resolved PL (TRPL) measurements (Figure 3d). PL intensity decays via the recombination of excited charge carriers. Figure 3d showed that the decay of PL intensity was slowed by ZnS deposition compared with that of bare CIGS film, suggesting that a ZnS coating can suppress the recombination process on the CIGS surface. The hump in the TRPL spectra of bare CIGS at around 2.5 ns is due to the instrumental internal response function which can be observed when the lifetime of the semiconductor is short.[44] The TRPL results suggested that the ZnS layer can effectively passivate the CIGS surface.

In addition, the ZnS layer improved the stability of the CIGS photocathode by protecting the bottom of the CIGS semiconductor film from the photo/dark corrosion reaction.[35] The photocurrent of the CIGS/Pt photoelectrode gradually diminished to only 25% of the initial photocurrent after 3 h (Figure 4). CIGS/ZnS/Pt exhibited a more stable photocurrent, although it was also slowly deactivated. The more

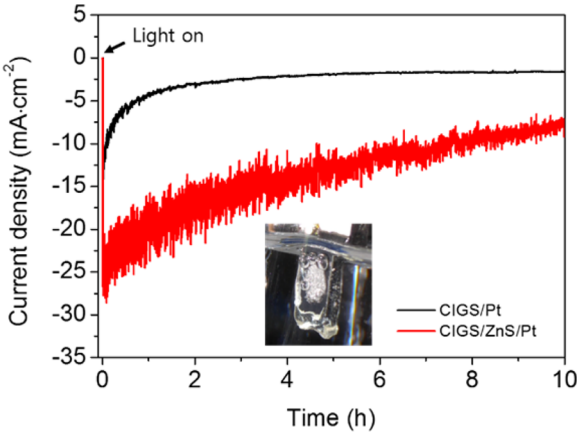

Figure 4. $I-t$ graph of CIGS/ZnS/Pt under simulated sunlight at −0.5 V vs RHE. Inset photograph shows hydrogen bubble evolution on photoelectrode surface.

DOI: 10.1021/jacs.6b09595
J. Am. Chem. Soc. 2016, 138, 15673−15681

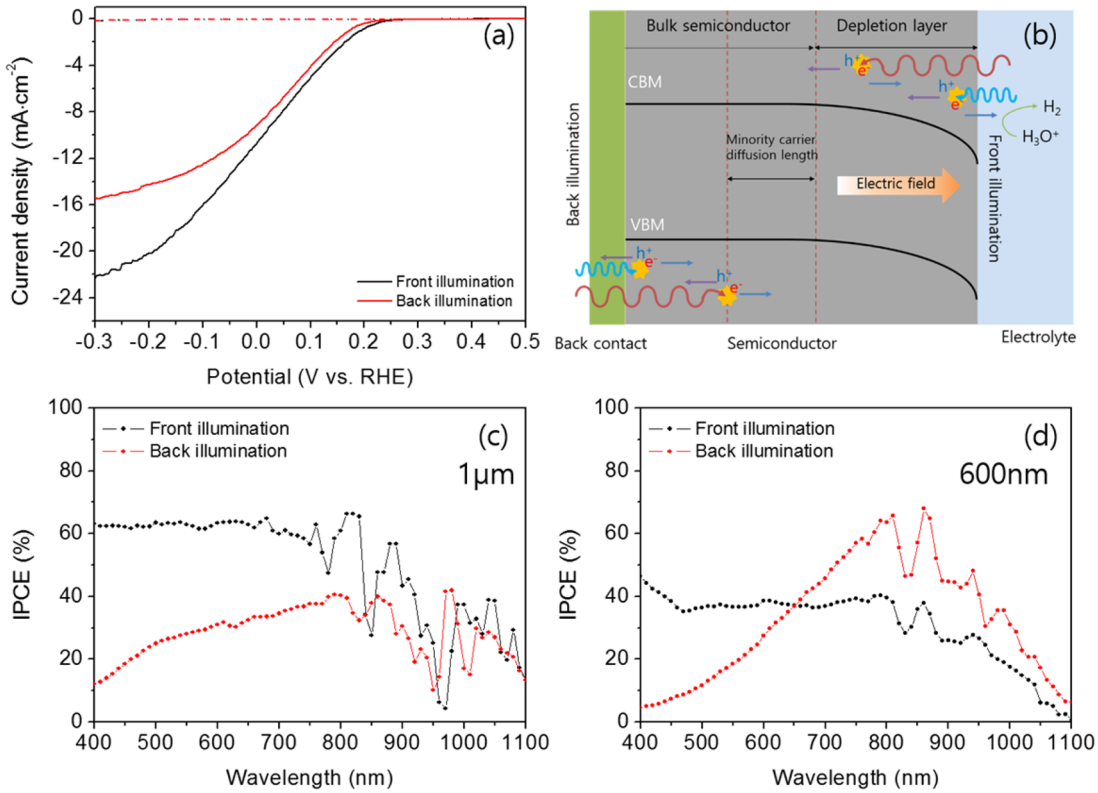

Figure 5. (a) *I*−*V* curve measurements of a CIGS/ZnS/Pt photocathode with 1 μm CIGS thickness depending on the illumination directions; front illumination (black solid line), and back illumination (red solid line). Dotted lines were measured in dark condition. (b) Schematic diagram of charge flows under front/back illumination. IPCE measurements at −0.5 V vs Ag/AgCl of a CIGS/ZnS/Pt photocathode depending on the illumination directions; with (c) 1 μm CIGS thin film, and (d) 600 nm CIGS thin film.

severe degradation was observed with the CIGS/Pt photocathode after the PEC reaction according to the SEM images and EDS analysis (Figure S8, Supporting Information). To prolong the stability of the CIGS photocathode, it is required to develop a better protection layer and increase Pt adhesion on the surface. We also determined whether the photocurrent was indeed used in the evolution of hydrogen from water using GC analysis of the gaseous products during chronoamperometry measurements (Figure S9, Supporting Information). The average Faradaic efficiency (or current efficiency) was ∼94%, confirming that most of the electrons that passed through the CIGS photocathode were used in the hydrogen evolution reaction (HER).

In addition to the surface states, electron and hole transportation within the semiconductor layer is an important factor affecting PEC performance. Charge separation efficiency can decrease in thicker film because electrons and holes have a higher chance of recombination as they travel a longer distance to the surface or the back contact. In addition to film thickness, the direction of illumination (i.e., front or back illumination) for the photoelectrode can alter charge separation efficiency. Because our CIGS film was prepared on a transparent FTO substrate instead of the conventional opaque Mo film, we were able to compare the effect of front and back illumination on PEC activity, which can provide more information on the viability of tandem structures where CIGS photocathodes are stacked on other semiconductors.

The photocurrent density of ∼1 μm thin CIGS/ZnS/Pt photocathodes showed the lower PEC activity under back illumination (toward FTO/CIGS) compared to front (toward Pt/ZnS/CIGS) one (Figure 5a). A drop of the IPCE values at the shorter wavelength regions was observed only under back illumination (Figure 5c). With normal front illumination, IPCE values are more or less similar where the wavelength (λ) is shorter than 800 nm while decreasing as the wavelength increases. A sharp decrease of the IPCE values at the IR region can be attributed to light absorption by water molecules.[45]

IPCE is affected by the light absorption efficiency, charge transport efficiency to the semiconductor-electrolyte interface, and interfacial charge transfer efficiency across the electrolyte. In a comparison with the UV−vis absorbance spectra (Figure 1f), we found that the relationship between IPCE values and wavelength followed the trend of the absorbance spectra, indicating that light absorption efficiency is crucial for our CIGS photocathodes under front illumination. In the shorter wavelength regions (λ < 800 nm), similar IPCE values suggest that 1 μm CIGS film is thick enough to absorb most of the incident light. We calculated the absorption coefficient and the penetration depth (Figure S10, Supporting Information) of the synthesized CIGS absorber from the measured UV−vis absorption spectra. Penetration depth measures how far the light reaches into the semiconductor before being absorbed and can be calculated from the reciprocal of the absorption coefficient.[51]

The incident light (λ < 800 nm) has a much shorter penetration depth (<300 nm) than the film thickness of 1 μm (Figure S10b, Supporting Information). However, the IPCE values were saturated at 60−65%. One possible explanation for the loss of quantum efficiency is reduced absorption at the photoelectrode surface due to reflection or scattering.

DOI: 10.1021/jacs.6b09595
J. Am. Chem. Soc. 2016, 138, 15673−15681

According to the UV−vis spectra, we found that the maximum light absorption was ∼80% at λ < 800 nm (Figure 1f). The other possible reason is recombination loss; if the electron lifetime is shorter than the water reduction kinetics, the electrons would recombine with holes at this interface. Although our ZnS layer helps to suppress charge recombination at the CIGS surface, the IPCE values indicate that further improvement is required. On the other hand, the IPCE values gradually decreased at longer wavelength regions (λ > 800 nm) as the absorption efficiency decreases for light at longer wavelengths.

According to the Gärtner model,[52] when incident light is absorbed near the surface within the depletion layer and the minority carrier diffusion length, the carriers can be efficiently separated due to drift under the electric field. However, incident light with longer wavelengths can be absorbed and excite electrons outside of the depletion layer, which impairs charge transport efficiency due to recombination loss (Figure 5b). The loss of quantum efficiency caused by electron transport was more serious when the light irradiated the back side of the photocathode, especially for shorter wavelength regions (Figure 5c). In our CIGS film, the penetration depths were around 140, 170, and 530 nm for 350, 600, and 900 nm wavelength light, respectively, which means that, for the shorter wavelength, the more photons were absorbed near the back of the CIGS film. When the photons are absorbed near the FTO−CIGS interface, a long way from the depletion layer, the minority carrier electrons are vulnerable to recombination with holes because the electrons have to travel long distance to the semiconductor/liquid interface where the HER reaction occurs. Therefore, longer penetration depth is more favorable for back side illumination, and higher IPCE values are obtained with longer wavelength lights in 400 < λ < 850 nm region. Based on our back side illumination experiment, it was found that the depletion layer of our solution-processed CIGS film was shorter than the film thickness (d = 1 μm), causing a significant loss of charge transport.

When we conducted the same experiment with thinner CIGS films of d = 400−800 nm (Figure S11), increasing IPCE values were again observed as wavelength increased from λ = 400 to 850 nm region when the light came from the back side of the photoelectrode. Figure 5d showed the IPCE values of d = 600 nm thin CIGS film were even higher for longer wavelength regions (λ > 650 nm) under back illumination compared to front illumination. In contrast, 1 μm thin CIGS photocathodes always produced smaller or similar IPCE values under back illumination (Figure. 5c). An inversion of IPCE values can occur for thinner film when more photons with long wavelengths are absorbed close to the depletion layer, thus increasing the electron transport efficiency compared to front illumination (Figure S10c, Supporting Information). Also, we found that minority carrier (electron) transport is critical for efficient charge transport in CIGS photocathodes. If majority hole transport was more important, higher IPCE values should be obtained at shorter wavelengths under back illumination because the excited holes are close to the back contact, but we observed the opposite result. This dependence of quantum efficiency on the direction of illumination may be useful when designing tandem photoelectrochemical cells and determining whether to use front or back illumination.

CONCLUSIONS

In this study, Cu(In,Ga)(S,Se)$_2$ (CIGS) thin film was prepared on a transparent FTO substrate using a solution-based method for photoelectrochemical water reduction. Its photocurrent was greatly improved, proving to be as active as CIGS thin film prepared by the vacuum process. Further improvement of the photocurrent was achieved by coating ZnS on the CIGS thin film, which acted as a passivation layer. In addition, when the incident light illuminated the back side of the CIGS photocathode, a decrease in quantum efficiency was observed for shorter wavelengths, indicating that fast electron transportation toward the CIGS/electrolyte interface is important for increasing charge separation efficiency. This cost-effective, highly active, and semitransparent CIGS photocathode will be useful for application in solar water splitting cells, especially those with a tandem structure.

ASSOCIATED CONTENT

Supporting Information

The Supporting Information is available free of charge on the ACS Publications website at DOI: 10.1021/jacs.6b09595.

XRD, SEM and XPS spectra data of CIGS, additional Mott−Schottky analysis and PL data for CIGS photoelectrode and Absorption coefficient and penetration depth data (PDF)

AUTHOR INFORMATION

Corresponding Authors

*bkmin@kist.re.kr

*yjhwang@kist.re.kr

Notes

The authors declare no competing financial interest.

ACKNOWLEDGMENTS

This work was supported by Korea Institute of Science and Technology (KIST) Institutional Program and it was partly supported by the University-Institute Cooperation Program of the National Research Foundation of Korea funded by the Korean Government (MSIP). We thanks M. S. Jee for helpful discussions.

REFERENCES

(1) Fujishima, A.; Honda, K. *Nature* **1972**, *238*, 37−38.

(2) Hung, S.-F.; Xiao, F.-X.; Hsu, Y.-Y.; Suen, N.-T.; Yang, H.-B.; Chen, H. M.; Liu, B. *Adv. Energy Mater.* **2016**, *6*, 1501339.

(3) Xiao, F.-X.; Zeng, Z.; Liu, B. *J. Am. Chem. Soc.* **2015**, *137*, 10735−10744.

(4) Paracchino, A.; Laporte, V.; Sivula, K.; Grätzel, M.; Thimsen, E. *Nat. Mater.* **2011**, *10*, 456−461.

(5) Hisatomi, T.; Kubota, J.; Domen, K. *Chem. Soc. Rev.* **2014**, *43*, 7520−7535.

(6) Huang, Q.; Kang, F.; Liu, H.; Li, Q.; Xiao, X. *J. Mater. Chem. A* **2013**, *1*, 2418−2425.

(7) Liao, M.; Feng, J.; Luo, W.; Wang, Z.; Zhang, J.; Li, Z.; Yu, T.; Zou, Z. *Adv. Funct. Mater.* **2012**, *22*, 3066−3074.

(8) Prévot, M. S.; Sivula, K. *J. Phys. Chem. C* **2013**, *117*, 17879−17893.

(9) Kaneko, H.; Minegishi, T.; Nakabayashi, M.; Shibata, N.; Kuang, Y.; Yamada, T.; Domen, K. *Adv. Funct. Mater.* **2016**, *26*, 4570−4577.

(10) Kim, J. H.; Kaneko, H.; Minegishi, T.; Kubota, J.; Domen, K.; Lee, J. S. *ChemSusChem* **2016**, *9*, 61−66.

(11) Yang, H. B.; Miao, J.; Hung, S.-F.; Huo, F.; Chen, H. M.; Liu, B. *ACS Nano* **2014**, *8*, 10403−10413.

DOI: 10.1021/jacs.6b09595
J. Am. Chem. Soc. 2016, 138, 15673−15681

(12) Kim, J. Y.; Magesh, G.; Youn, D. H.; Jang, J.-W.; Kubota, J.; Domen, K.; Lee, J. S. *Sci. Rep.* **2013**, *3*, 2681.
(13) Zhong, M.; Hisatomi, T.; Kuang, Y.; Zhao, J.; Liu, M.; Iwase, A.; Jia, Q.; Nishiyama, H.; Minegishi, T.; Nakabayashi, M.; Shibata, N.; Niishiro, R.; Katayama, C.; Shibano, H.; Katayama, M.; Kudo, A.; Yamada, T.; Domen, K. *J. Am. Chem. Soc.* **2015**, *137*, 5053−5060.
(14) Kim, T. W.; Choi, K.-S. *Science* **2014**, *343*, 990−994.
(15) Kibria, M. G.; Chowdhury, F. A.; Zhao, S.; AlOtaibi, B.; Trudeau, M. L.; Guo, H.; Mi, Z. *Nat. Commun.* **2015**, *6*, 6797.
(16) Young, J. L.; Steirer, K. X.; Dzara, M. J.; Turner, J. A.; Deutsch, T. G. *J. Mater. Chem. A* **2016**, *4*, 2831−2836.
(17) Lee, M. H.; Takei, K.; Zhang, J.; Kapadia, R.; Zheng, M.; Chen, Y.-Z.; Nah, J.; Matthews, T. S.; Chueh, Y.-L.; Ager, J. W.; Javey, A. *Angew. Chem., Int. Ed.* **2012**, *51*, 10760−10764.
(18) Tinoco, T.; Rincón, C.; Quintero, M.; Pérez, G. S. *Phys. Status Solidi A* **1991**, *124*, 427−434.
(19) Stanbery, B. J. *Crit. Rev. Solid State Mater. Sci.* **2002**, *27*, 73−117.
(20) Jacobsson, T. J.; Platzer-Björkman, C.; Edoff, M.; Edvinsson, T. *Int. J. Hydrogen Energy* **2013**, *38*, 15027−15035.
(21) Kumagai, H.; Minegishi, T.; Sato, N.; Yamada, T.; Kubota, J.; Domen, K. *J. Mater. Chem. A* **2015**, *3*, 8300−8307.
(22) Luo, J.; Li, Z.; Nishiwaki, S.; Schreier, M.; Mayer, M. T.; Cendula, P.; Lee, Y. H.; Fu, K.; Cao, A.; Nazeeruddin, M. K.; Romanyuk, Y. E.; Buecheler, S.; Tilley, S. D.; Wong, L. H.; Tiwari, A. N.; Grätzel, M. *Adv. Energy Mater.* **2015**, *5*, 1501520.
(23) Guijarro, N.; Prévot, M. S.; Yu, X.; Jeanbourquin, X. A.; Bornoz, P.; Bourée, W.; Johnson, M.; Le Formal, F.; Sivula, K. A *Adv. Energy Mater.* **2016**, *6*, 1501949.
(24) Mandati, S.; Sarada, B. V.; Dey, S. R.; Joshi, S. V. *Electron. Mater. Lett.* **2015**, *11*, 618−624.
(25) Guan, Z.; Luo, W.; Feng, J.; Tao, Q.; Xu, Y.; Wen, X.; Fu, G.; Zou, Z. *J. Mater. Chem. A* **2015**, *3*, 7840−7848.
(26) Hibberd, C. J.; Chassaing, E.; Liu, W.; Mitzi, D. B.; Lincot, D.; Tiwari, A. N. *Prog. Photovoltaics* **2010**, *18*, 434−452.
(27) Kemell, M.; Ritala, M.; Leskelä, M. *Crit. Rev. Solid State Mater. Sci.* **2005**, *30*, 1−31.
(28) Yokoyama, D.; Minegishi, T.; Maeda, K.; Katayama, M.; Kubota, J.; Yamada, A.; Konagai, M.; Domen, K. *Electrochem. Commun.* **2010**, *12*, 851−853.
(29) Park, S. J.; Jeon, H. S.; Cho, J. W.; Hwang, Y. J.; Park, K. S.; Shim, H. S.; Song, J. K.; Cho, Y.; Kim, D.-W.; Kim, J.; Min, B. K. *ACS Appl. Mater. Interfaces* **2015**, *7*, 27391−27396.
(30) Turcu, M.; Rau, U. *Thin Solid Films* **2003**, *431*−*432*, 158−162.
(31) Hiroshi, O.; Hiroshi, M.; Kazuhiko, Y. *Jpn. J. Appl. Phys.* **1982**, *21*, 1075.
(32) Chazalviel, J. N. *Surf. Sci.* **1979**, *88*, 204−220.
(33) Madou, M. J.; Loo, B. H.; Frese, K. W.; Morrison, S. R. *Surf. Sci.* **1981**, *108*, 135−152.
(34) Romanyuk, Y. E.; Hagendorfer, H.; Stücheli, P.; Fuchs, P.; Uhl, A. R.; Sutter-Fella, C. M.; Werner, M.; Haass, S.; Stückelberger, J.; Broussillou, C.; Grand, P.-P.; Bermudez, V.; Tiwari, A. N. *Adv. Funct. Mater.* **2015**, *25*, 12−27.
(35) Liu, R.; Zheng, Z.; Spurgeon, J.; Yang, X. *Energy Environ. Sci.* **2014**, *7*, 2504−2517.
(36) Guijarro, N.; Campina, J. M.; Shen, Q.; Toyoda, T.; Lana-Villarreal, T.; Gomez, R. *Phys. Chem. Chem. Phys.* **2011**, *13*, 12024−12032.
(37) Diguna, L. J.; Shen, Q.; Kobayashi, J.; Toyoda, T. *Appl. Phys. Lett.* **2007**, *91*, 023116.
(38) Chen, Y.; Tao, Q.; Fu, W.; Yang, H.; Zhou, X.; Zhang, Y.; Su, S.; Wang, P.; Li, M. *Electrochim. Acta* **2014**, *118*, 176−181.
(39) Hsu, Y.-J.; Lu, S.-Y. *Langmuir* **2004**, *20*, 194−201.
(40) Hwang, J.-Y.; Park, S. Y.; Park, J.-H.; Kim, J.-N.; Koo, S. M.; Ko, C. H. *Thin Solid Films* **2012**, *520*, 1832−1836.
(41) Weinhardt, L.; Fuchs, O.; Peter, A.; Umbach, E.; Heske, C.; Reichardt, J.; Bär, M.; Lauermann, I.; Kötschau, I.; Grimm, A.; Sokoll, S.; Lux-Steiner, M. C.; Niesen, T. P.; Visbeck, S.; Karg, F. *J. Chem. Phys.* **2006**, *124*, 074705.
(42) Barreca, D.; Tondello, E.; Lydon, D.; Spalding, T. R.; Fabrizio, M. *Chem. Vap. Deposition* **2003**, *9*, 93−98.
(43) Barreca, D.; Gasparotto, A.; Maragno, C.; Tondello, E.; Spalding, T. R. *Surf. Sci. Spectra* **2002**, *9*, 54−61.
(44) Park, Y. S.; Im, H.; Yoon, I. T.; Lee, S. K.; Cho, Y. H.; Taylor, R. A. *J. Korean Phys. Soc.* **2010**, *57*, 756−759.
(45) Doscher, H.; Geisz, J. F.; Deutsch, T. G.; Turner, J. A. *Energy Environ. Sci.* **2014**, *7*, 2951−2956.
(46) Septina, W.; Gunawan; Ikeda, S.; Harada, T.; Higashi, M.; Abe, R.; Matsumura, M. *J. Phys. Chem. C* **2015**, *119*, 8576−8583.
(47) Zhao, J.; Minegishi, T.; Zhang, L.; Zhong, M.; Gunawan; Nakabayashi, M.; Ma, G.; Hisatomi, T.; Katayama, M.; Ikeda, S.; Shibata, N.; Yamada, T.; Domen, K. *Angew. Chem., Int. Ed.* **2014**, *53*, 11808−11812.
(48) Azarpira, A.; Lublow, M.; Steigert, A.; Bogdanoff, P.; Greiner, D.; Kaufmann, C. A.; Krüger, M.; Gernert, U.; van de Krol, R.; Fischer, A.; Schedel-Niedrig, T. *Adv. Energy Mater.* **2015**, *5*, 1402148.
(49) Ros, C.; Andreu, T.; Giraldo, S.; Sánchez, Y.; Morante, J. R. *Sol. Energy Mater. Sol. Cells* **2016**, *158*, 184−188.
(50) Mali, M. G.; Yoon, H.; Joshi, B. N.; Park, H.; Al-Deyab, S. S.; Lim, D. C.; Ahn, S.; Nervi, C.; Yoon, S. S. *ACS Appl. Mater. Interfaces* **2015**, *7*, 21619−21625.
(51) Sridhara, S. G.; Devaty, R. P.; Choyke, W. J. *J. Appl. Phys.* **1998**, *84*, 2963−2964.
(52) Gärtner, W. W. *Phys. Rev.* **1959**, *116*, 84−87.

DOI: 10.1021/jacs.6b09595
J. Am. Chem. Soc. 2016, 138, 15673−15681